

Revised on June 11, 2018

# Impact of Charge Ordering on Magnetic Correlations in Perovskite (Bi,Ca)MnO<sub>3</sub>

Wei Bao,<sup>1</sup> J. D. Axe,<sup>1</sup> C. H. Chen<sup>2</sup> and S-W. Cheong<sup>2</sup><sup>1</sup>*Brookhaven National Laboratory, Upton, NY 11973*<sup>2</sup>*Bell Laboratories, Lucent Technologies, Murray Hill, NJ 07974*

## Abstract

Single crystalline Bi<sub>1-x</sub>Ca<sub>x</sub>MnO<sub>3</sub> ( $0.74 \leq x \leq 0.82$ ) were studied with neutron scattering, electron diffraction and bulk magnetic measurement. We discovered dynamic ferromagnetic spin correlations at high temperatures, which are replaced by antiferromagnetic spin fluctuations at a concomitant charge ordering and structural transition. Our results indicate that thermal-activated hopping of the Jahn-Teller active  $e_g$  electrons in these insulating materials, nevertheless, induce ferromagnetic interaction through double-exchange mechanism. It is the ordering of these charges competing with the double-exchange ferromagnetic metallic state.

Typeset using REVTeX

The relation between double exchange and Jahn-Teller distortion is one of the central issues [1] in current research on perovskite mixed-valent manganites  $T_{1-x}D_x\text{MnO}_3$  ( $T$  being trivalent ions, e.g., La, Pr or Nd, and  $D$  being divalent ions, e.g., Ca, Sr, Ba or Pb [2]). In these materials, the mean number of  $3d$  electrons per Mn can be tuned from 4 to 3. Due to strong Hund rule coupling,  $\text{Mn}^{3+}$  has a high-spin state  $t_{2g}^3e_g^1$  and the  $e_g$  level is split by Jahn-Teller distortion. For the  $\text{Mn}^{3+}$ -end members, the long range order of the elongated  $\text{MnO}_6$  octahedra (with  $d_{z^2}$ -type orbitals for this kind of Jahn-Teller distortion) stabilizes an insulating antiferromagnetic ground state [3–5]. In doped samples,  $e_g$  electron hopping [6] between  $\text{Mn}^{3+}$  and  $\text{Mn}^{4+}$  neighbor induces ferromagnetic correlations through the so-called double exchange mechanism [7]. It is well known that for  $x$  larger than a threshold value, a ferromagnetic metallic ground state becomes stable [8,9]. A structural transition to a higher symmetry state also occurs at the threshold [10], which results from the ability of the hopping  $e_g$  electrons to destroy the long range coherence of the Jahn-Teller distortion (or  $d_{z^2}$ -type orbitals) [4]. Long range order of charges in the  $\text{Mn}^{4+}(t_{2g}^3)$ -rich regime was recently observed with electron diffraction in  $\text{La}_{1-x}\text{Ca}_x\text{MnO}_3$  ( $x > 0.5$ ) [11]. A large anomaly in sound velocity was found at the charge ordering temperature. More interestingly, the magnetic susceptibility  $\chi(T)$  has a pronounced inflection at the charge ordering temperature, resembling that associated with a conventional long range antiferromagnetic transition [12]. However, thermodynamic measurements suggest that the antiferromagnetic order develops at a lower temperature [11]. In order to clarify and understand the anomalous lattice and magnetic phenomena at charge ordering, microscopic information is crucial, and neutron scattering is the ideal probe for this purpose with its access to static and dynamic correlations of both magnetic and structural degrees of freedom [13].

Single crystals of  $\text{La}_{1-x}\text{Ca}_x\text{MnO}_3$  ( $x > 0.5$ ) are not available. However, we have succeeded in growing single crystals of isostructural  $\text{Bi}_{1-x}\text{Ca}_x\text{MnO}_3$  in this  $\text{Mn}^{4+}$ -rich regime. As the following description will show,  $(\text{Bi,Ca})\text{MnO}_3$  bears close resemblance to  $(\text{La,Ca})\text{MnO}_3$  in the overlapping composition range, attesting to the identical underlying physics. Single crystals of  $(\text{Bi,Ca})\text{MnO}_3$ , however, allow us to extract much more infor-

mation with neutron scattering. We found that the charge ordering is accompanied by a structural transition and that antiferromagnetic long range order indeed develops at a lower temperature. The most important of our discoveries, however, is that the nature of spin fluctuations change from *ferromagnetic* to *antiferromagnetic* at the charge ordering transition. These results indicate that at high temperatures, thermally activated  $e_g$  electron hopping in the insulating regime, nevertheless, induces ferromagnetic correlations through the double-exchange mechanism. When  $e_g$  electrons with their accompanying Jahn-Teller distortions freeze in static order, the double exchange induced ferromagnetic spin fluctuations are replaced by superexchange antiferromagnetic spin fluctuations.

Single crystals of  $\text{Bi}_{1-x}\text{Ca}_x\text{MnO}_3$  were grown using the flux method. The compositions of samples were determined by inductive coupled plasma emission spectroscopy. The weights of samples used in neutron scattering are 25, 127 and 320mg for  $x=0.74$ , 0.76 and 0.82, respectively. Charge ordering was observed with electron diffraction using a JOEL 2000FX transmission electron microscope. Superlattice peaks with wave vector  $(\delta, 0, 0)$  in  $Pbnm$  notation appear below a charge ordering temperature,  $T_O$ , similar to those in  $(\text{La,Ca})\text{MnO}_3$  [11].  $\delta \simeq 0.30$  and 0.22 for  $x = 0.74$  and 0.82, respectively. The decreasing  $\delta$  is consistent with the decreasing numbers of  $e_g$  electrons, which are involved in the charge ordering. Fig. 1(a) shows the development of the charge superlattice intensity of  $(0.22, 0, 0)$  below  $T_O = 210\text{K}$  for a  $x=0.82$  sample. Magnetic susceptibility was measured for crystals from the same batches with a Quantum Design SQUID magnetometer. Consistent results were found for different crystals from the same batch. Fig. 1(b) shows an example for  $x=0.82$ . At high temperatures, the Curie-Weiss law is followed, yielding an effective moment  $p = 4.15(2)\mu_B$  which is close to the expected  $p = 4.08$  for this composition. The positive value of the Weiss constant  $\Theta = 159(1)\text{K}$  reveals the existence of ferromagnetic correlations between Mn spins. The drastic reduction of  $\chi(T)$  at the charge ordering temperature,  $T_O$ , is similar to that observed in  $(\text{La,Ca})\text{MnO}_3$  [12]. At 160K, there begins a further reduction in the magnetic susceptibility, whose origin will become clear after the presentation of our neutron scattering results.

Neutron scattering experiments were conducted with triple axis spectrometers at the HFBR at Brookhaven National Laboratory. Except for polarized neutron scattering, graphite monochromators and analyzers were used. High order contaminations were removed with graphite filters. At room temperature, the selection rules for nuclear Bragg peaks are consistent with space group  $Pbnm$ . However, the orthorhombic distortion is small. For the purpose of this paper, we use the simpler pseudocubic perovskite unit cell [14]. Fig. 1(c) shows the pseudocubic lattice parameters as a function of temperature for a  $x=0.82$  sample. At the charge ordering temperature  $T_O$ , there is a structural transition, as evidenced by the splitting of the Bragg peaks. This result is not totally surprising, since each  $e_g$  electron carries with it a Jahn-Teller lattice distortion. When  $e_g$  electrons order, long range correlations can develop among Jahn-Teller distorted  $MnO_6$  octahedra [4].

In a pioneering powder neutron diffraction study, three types of magnetic structures were reported in the composition range  $0.74 \leq x \leq 0.82$  for  $La_{1-x}Ca_xMnO_3$  [3]. We have conducted thorough search in (hk0) and (hhl) zones of (Bi,Ca) $MnO_3$  at low temperatures. For all of our samples, magnetic Bragg peaks are found only at C-type points,  $(\frac{2n+1}{2}, \frac{2m+1}{2}, l)$ . We distinguished magnetic peaks from structural superlattice peaks not only with temperature dependence, but more conclusively using polarized neutron scattering. Heusler crystals were used both as monochromator and analyzer, and a spin flipper and a graphite filter were placed in the diffracted beam. The inset on the right of Fig. 1(d) shows an example of a  $(1/2, 1/2, 0)$  scan for the  $x=0.82$  sample. By aligning a magnetic field along different directions at the sample position, the magnetic nature of the Bragg peak is proven and the spin direction is determined [15]. In the current case, spin lies along the c-axis, as found in (La,Ca) $MnO_3$  for a C-type antiferromagnet [3]. The resulting spin structure is shown in the left insert to Fig. 1(d). Possible implications of this magnetic structure for  $e_g$  orbital ordering has been discussed by Goodenough [4]. Comparing the magnetic and nuclear Bragg intensities, the staggered magnetic moment at 9K is determined to be  $3.5(2)\mu_B$  per Mn. This corresponds to an average Mn spin  $S = 1.8(1)$  and  $p = 2\sqrt{S(S+1)} = 4.4(3)$  is in good agreement with that given by susceptibility measurement at high temperatures. The

temperature dependence of the order parameter in Fig. 1(d) establishes the Néel temperature  $T_N = 160\text{K}$  for  $x = 0.82$  which coincides with the lower inflection point of  $\chi(T)$  in Fig. 1(b). The Néel temperature  $T_N$  and the charge-structural transition temperature  $T_O$  for various samples are summarized in the insert to Fig. 1(a). This phase diagram parallels that of  $(\text{La,Ca})\text{MnO}_3$  [11], pointing to a generic behavior for both systems.

After establishing the phase relation and the magnetic ground state, let us now turn to dynamic spin properties. Fig. 2(a) shows spin-wave dispersion along three symmetry directions for  $x = 0.82$  measured at 11K near a magnetic zone center. The spin Hamiltonian which describes Mn spins below charge ordering transition is

$$\mathcal{H} = \sum_{\langle i,j \rangle_{AF}} J_{AF} \mathbf{S}_i \cdot \mathbf{S}_j + \sum_{\langle i,j \rangle_F} J_F \mathbf{S}_i \cdot \mathbf{S}_j - g\mu_B H_u \sum_i |S_i^z|$$

where  $J_{AF}$  and  $J_F$  are antiferromagnetic and ferromagnetic nearest neighbors interactions (refer to Fig. 1(d)) and  $H_u$  is a uniaxial anisotropy field. Each nearest neighbor spin pair is counted only once in the summations. Conventional spin wave theory yields the dispersion relation [13]

$$\hbar\omega(\mathbf{q}) = \sqrt{[\mathcal{J}(0) - \mathcal{J}_1(0) + \mathcal{J}_1(\mathbf{q}) + g\mu_B H_u]^2 - \mathcal{J}(\mathbf{q})^2} \quad (1)$$

where  $\mathbf{q} = (hkl)$  is the wave vector from an antiferromagnetic zone center,  $\mathcal{J}(\mathbf{q}) = 2SJ_{AF}(\cos(2\pi h) + \cos(2\pi k))$  and  $\mathcal{J}_1(\mathbf{q}) = 2SJ_F \cos(2\pi l)$ . This dispersion relation accounts well for our data, as indicated by the solid curves in Fig. 2(a). From the fit we derive  $SJ_{AF} = 3.6(1)\text{meV}$ ,  $SJ_F = -1.3(1)\text{meV}$  and  $H_u = 4.4(3)\text{T}$ . The zone boundary energy at  $(0,0,1/2)$  derived using these parameters is  $13.8(8)\text{meV}$ , which corresponds nicely to the observed  $k_B T_N$  as expected for a bi-partite 3-dimensional magnet. Recently, the spin wave dispersion has been measured for ferromagnetic samples [16–18]. A Heisenberg nearest neighbor model describes well the experimental results at low temperatures. The nearest neighbor exchange varies from  $SJ = -12.6(5)\text{meV}$  at 27K to  $-7.6(3)\text{meV}$  at 300K for  $\text{La}_{0.7}\text{Sr}_{0.3}\text{MnO}_3$  [16]; for  $\text{La}_{0.7}\text{Pb}_{0.3}\text{MnO}_3$  and  $\text{La}_{0.77}\text{Ca}_{0.33}\text{MnO}_3$ , the corresponding value at  $T \rightarrow 0$  is  $-8.8(2)\text{meV}$  [17] and  $-11.4\text{meV}$  [18], respectively. Ferromagnetic double-exchange

in these samples appears to be stronger than the antiferromagnetic superexchange measured in our sample [22].

There is an energy gap  $\Delta = 3.8\text{meV}$  in the spin wave excitations of Fig. 2(a). Compared with  $k_B T_N = 13.8\text{meV}$ , this is a very large spin gap. Similar spin gaps were also found for  $x = 0.74$  and  $0.76$  samples. A constant  $\mathbf{q}$  scan for  $x = 0.76$  at  $(1/2, 1/2, 0)$  is shown in Fig. 2(b). This explains the pronounced reduction of  $\chi(T)$  below  $T_N$ . Similar, but less pronounced, reduction of  $\chi$  in the case of  $\text{La}_{1-x}\text{Ca}_x\text{MnO}_3$  ( $x > 0.5$ ) [11,12] is likely also to be caused by the development of a spin gap below  $T_N$ . The softening of the spin gap with elevated temperatures was measured and the results are shown in Fig. 2(b). We explain the spin gap in our insulating samples with uniaxial anisotropy. This could be a natural consequence of the ordering of the  $d_{z^2}$  orbitals. Meanwhile rapid hopping of  $d_{z^2}$  electrons in the metallic phase renders spin space isotropic and no gap in spin excitations is expected for the ferromagnetic manganites. This is indeed what was found experimentally for  $\text{La}_{0.77}\text{Ca}_{0.33}\text{MnO}_3$  with neutron scattering [18].

To investigate the anomalous reduction of  $\chi(T)$  at the charge-structural transition, we have directly measured dynamic spin correlations with inelastic neutron scattering. Antiferromagnetic spin fluctuations were probed at  $(1/2, 1/2, 0)$  (Fig. 3(b)) and ferromagnetic spin fluctuations near the forward direction (Fig. 3(c)), where magnetic form factor maximizes and structure factor for structural fluctuations diminishes as  $q^2$ . As charge order parameter grows below  $T_O$  (refer to Fig 1(a)), *ferromagnetic* spin fluctuations are replaced by *antiferromagnetic* spin fluctuations. This may be better seen in Fig. 3(a) which shows detail temperature variations of both the ferromagnetic response (circles, measured at  $\hbar\omega = 1\text{meV}$  and  $q = 0.17\text{\AA}$ ) and the antiferromagnetic response (disks, measured at  $\hbar\omega = 1.7\text{meV}$  and  $\mathbf{q} = (1/2, 1/2, 0)$ ). The absence of antiferromagnetic spin correlations above  $T_O$  is evidenced by a flat background both in the energy scan and in  $\mathbf{q}$  scans (refer to Fig. 3(b)) at  $(1/2, 1/2, 0)$ . The lower energy limit of this flat background was pushed down to  $0.4\text{meV}$  with better resolution of cold neutron scattering. There is obviously no any ferromagnetic component in the low temperature magnetic order (see Fig. 1(b)). This justifies our use of low tem-

perature data as the background for ferromagnetic response in Fig 3(a), and insert in (c) shows the net ferromagnetic intensity at 215K by subtracting background measured at 70K. Therefore our experimental results establish that ferromagnetic interactions exist between spins above  $T_O$  and they are replaced by antiferromagnetic interactions when charge orders. This switching of magnetic correlations from a ferromagnetic type to an antiferromagnetic type explains the inflection of  $\chi(T)$  at  $T_O$ .

A separate antiferromagnetic transition below a charge ordering transition was discovered previously in laminar perovskites  $\text{Sr}_{2-x}\text{La}_x\text{MnO}_4$  for  $x \sim 0.5$  [19]. This material also has an insulating antiferromagnetic ground state, and the high temperature ferromagnetic susceptibility is interrupted by charge ordering, as in the  $\text{Mn}^{4+}$ -rich  $(\text{La,Ca})\text{MnO}_3$  and  $(\text{Bi,Ca})\text{MnO}_3$ . Meanwhile, double exchange ferromagnetic ground state coincides with metallic conduction both in perovskite manganites for  $x \sim 0.3$  [20] and double layered  $(\text{La}_{0.4}\text{Sr}_{0.6})_3\text{Mn}_2\text{O}_7$  [21]. This suggests that the competition between double-exchange and the *ordering* of the Jahn-Teller active  $e_g$  electron is the dominant factor in determining the ground state of perovskite and related manganites.

In summary, we have observed directly in the  $\text{Mn}^{4+}$ -rich  $(\text{Bi,Ca})\text{MnO}_3$  a simultaneous charge ordering and structural transition. Above the charge-structural transition temperature  $T_O$ , there exist ferromagnetic spin fluctuations, indicative of double exchange induced by the  $e_g$  electron hopping. Below  $T_O$ , we discover the replacement of the ferromagnetic correlations by antiferromagnetic spin fluctuations, which support the notion that the ferromagnetic double-exchange diminishes as charge orders. The antiferromagnetic transition-like inflection point in  $\chi(T)$  at  $T_O$  is accounted for by this switch from ferromagnetic spin fluctuations to antiferromagnetic fluctuations. C-type long range antiferromagnetic order was found to develop in a separate phase transition at a lower temperature with large uniaxial anisotropy, which open a gap in spin excitations.

It is a pleasure to thank C. Broholm, S. M. Shapiro, G. Shirane, Q. Zhu, H. Y. Hwang, B. Batlogg, A. Zheludev, M. Martin and G. Y. Xu for discussions and assistances. WB acknowledges the Aspen Center for Physics where part of the work was performed. Work at

BNL was supported by DOE under Contract No. DE-AC02-76CH00016.



## REFERENCES

- [1] A. J. Millis, B. I. Shraiman and P. B. Littlewood, *Phys. Rev. Lett.* **74**, 5144 (1995).
- [2] J. B. Goodenough and J. M. Longon, in *Landolt-Börnstein, New Series III*, **4**, Pt a (Springer-Verlag, Berlin, 1970).
- [3] E. O. Wollan and W. C. Koehler, *Phys. Rev.* **100**, 545 (1955).
- [4] J. B. Goodenough, *Phys. Rev.* **100**, 564 (1955).
- [5] T. Mizokawa and A. Fujimori, *Phys. Rev. B* **51**, 12880 (1995); T. Saitoh et al., *ibid.* 13942 (1995).
- [6] Hopping of an  $e_g$  electron inevitably carries a Jahn-Teller lattice distortion with it. In other words, the charge motion is polaronic. We freely use  $e_g$  electron for this Jahn-Teller polaron in this paper.
- [7] C. Zener, *Phys. Rev.* **82**, 403 (1951); P. W. Anderson and H. Hasegawa, *ibid.* **100**, 675 (1955); P.-G. de Gennes, *ibid.* **118**, 141 (1960).
- [8] G. H. Jonker and J. H. Van Santen, *Physica* **16**, 337 (1950); J. H. Santen and G. H. Jonker, *ibid.* 599 (1950).
- [9] J.-H. Park, et al., *Phys. Rev. Lett.* **76** 4215 (1996).
- [10] G. Matsumoto, *J. Phys. Soc. Jpn.* **29**, 606; 615 (1970).
- [11] A. P. Ramirez, et al., *Phys. Rev. Lett.*, **76** 3188 (1996).
- [12] P. Schiffer, A. P. Ramirez, W. Bao and S-W. Cheong, *Phys. Rev. Lett.* **75** 3336, (1995).
- [13] S. W. Lovesey, *Theory of Neutron Scattering from Condensed Matter*, (Clarendon Press, Oxford, 1984).
- [14] Detail crystallographic study will be published separately. Q. Zhu *et al.*, (unpublished).

- [15] R. M. Moon, T. Riste, W. C. Koehler, Phys. Rev. **181**, 920 (1969). Finite counts for horizontal field with flipper off and vertical field with flipper on are due to imperfection of the polarizing instruments.
- [16] M. C. Martin, et al., Phys. Rev. B **53**, 14285 (1996).
- [17] T. G. Perring, et al., Phys. Rev. Lett. **76**, 711 (1996).
- [18] J. W. Lynn, et al., Phys. Rev. Lett. **76**, 4046 (1996).
- [19] W. Bao, C. H. Chen, S. A. Carter and S-W. Cheong, Solid State Comm. **98** 55, (1996).
- [20] R. M. Kusters, et al., Physica **B 155**, 362 (1989); K. Chahara, et al., Appl. Phys. Lett. **63**, 1990 (1993); H. L. Ju, et al., Phys. Rev. B **51**, 6143 (1995); A. Urushibara, et al., ibid. **51**, 14103 (1995); H. Y. Hwang, et al., Phys. Rev. Lett. **75**, 914 (1995).
- [21] Y. Moritomo, et al., Nature **380**, 141 (1996).
- [22] K. Hirota, et al., preprint (1996). Spin-wave excitations of A-type antiferromagnetic  $\text{LaMnO}_3$  was measured recently.  $SJ_F = -3.34(5)\text{meV}$ ,  $SJ_{AF} = 2.42(6)\text{meV}$  and  $H_u = 5.3(1)\text{T}$ .

## FIGURES

FIG. 1. Temperature dependences of (a) intensity of the charge superlattice peak, (b) magnetic susceptibility  $\chi$ , (c) pseudocubic lattice parameters, and (d) intensity of magnetic Bragg peak  $(1/2,1/2,0)$  for a  $x = 0.82$  sample.  $1/\chi$  (circles) is also shown in (b) with scale to the right and the straight line is a fit to the Curie-Weiss law. Polarized neutron scattering of  $(1/2,1/2,0)$  is shown in the right insert of (d): dots and circles are for the flipper turned off (Voff) and on (Von) cases with a magnetic field along  $(001)$ ; diamonds and squares for flipper off (Hoff) and on (Hon) with the magnetic field along the scattering wave vector. The spin structure determined is shown in the left corner of (d). Insert in (a): temperature-composition phase diagram for  $\text{Bi}_{1-x}\text{Ca}_x\text{MnO}_3$ , showing the charge-structural transition  $T_O$  (upper curve) and the Néel temperature  $T_N$  (lower curve).

FIG. 2. (a) Spin-wave dispersion along  $(110)$ ,  $(100)$  and  $(001)$  around the magnetic zone center  $(1/2,1/2,0)$ , measured at 11K for  $x = 0.82$ . The solid curves represent a fit to the spin-wave dispersion relation of Eq. (1). (b) Energy scans at  $(1/2,1/2,0)$  for  $x = 0.76$  at various temperatures. The energy gap,  $\Delta$ , of the spin excitations collapses when the Néel  $T_N = 130\text{K}$  is approached.

FIG. 3. (a) Temperature dependence of antiferromagnetic response measured at  $(1/2,1/2,0)$  and 1.7 meV (disks), and ferromagnetic response at  $|\mathbf{q}| = 0.17\text{\AA}^{-1}$  and 1 meV (circles) (marked with dashed lines in (b) and (c) respectively). The dotted line indicates background (see text for details). Below the charge ordering transition at  $T_O = 210\text{K}$ , ferromagnetic response is replaced by antiferromagnetic response (disks). (b) Energy scans at the antiferromagnetic zone center  $(1/2,1/2,0)$  at 165K (squares), 190K (disks), 220K (triangles) and 300K (diamonds). The solid line connects data at 300K which are indistinguishable from those at 220K. Insert shows constant  $\hbar\omega = 1.7\text{meV}$  scans at temperatures indicated. (c) Energy scans near the forward direction with  $|\mathbf{q}| = 0.17\text{\AA}^{-1}$ , probing ferromagnetic fluctuations, at 70K (squares), 215K (circles) and 300K (triangles). Insert shows 215K data with background at 70K subtracted, and the solid line is a Lorentzian.

Fig. 1, Wei Bao et al.

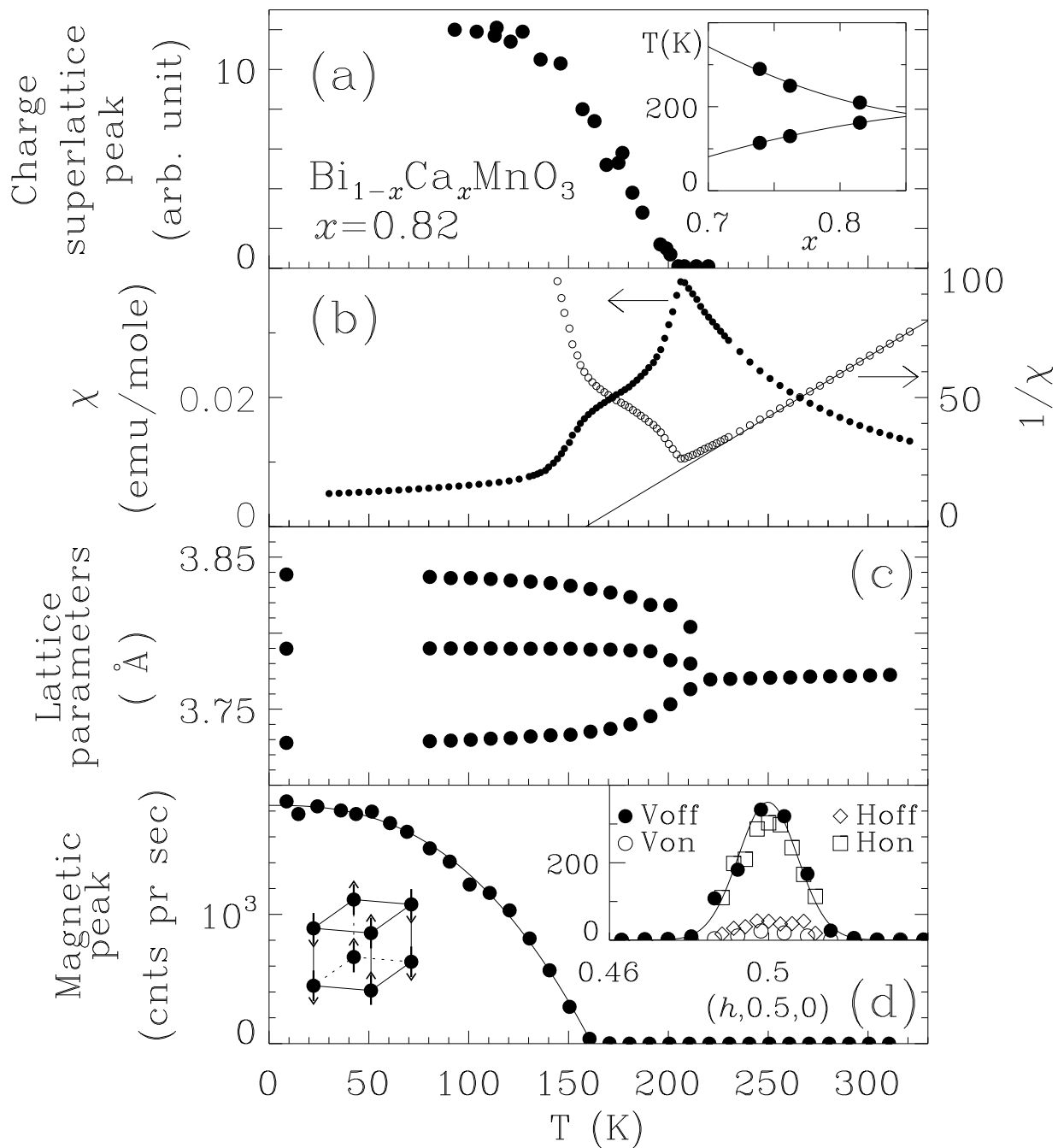
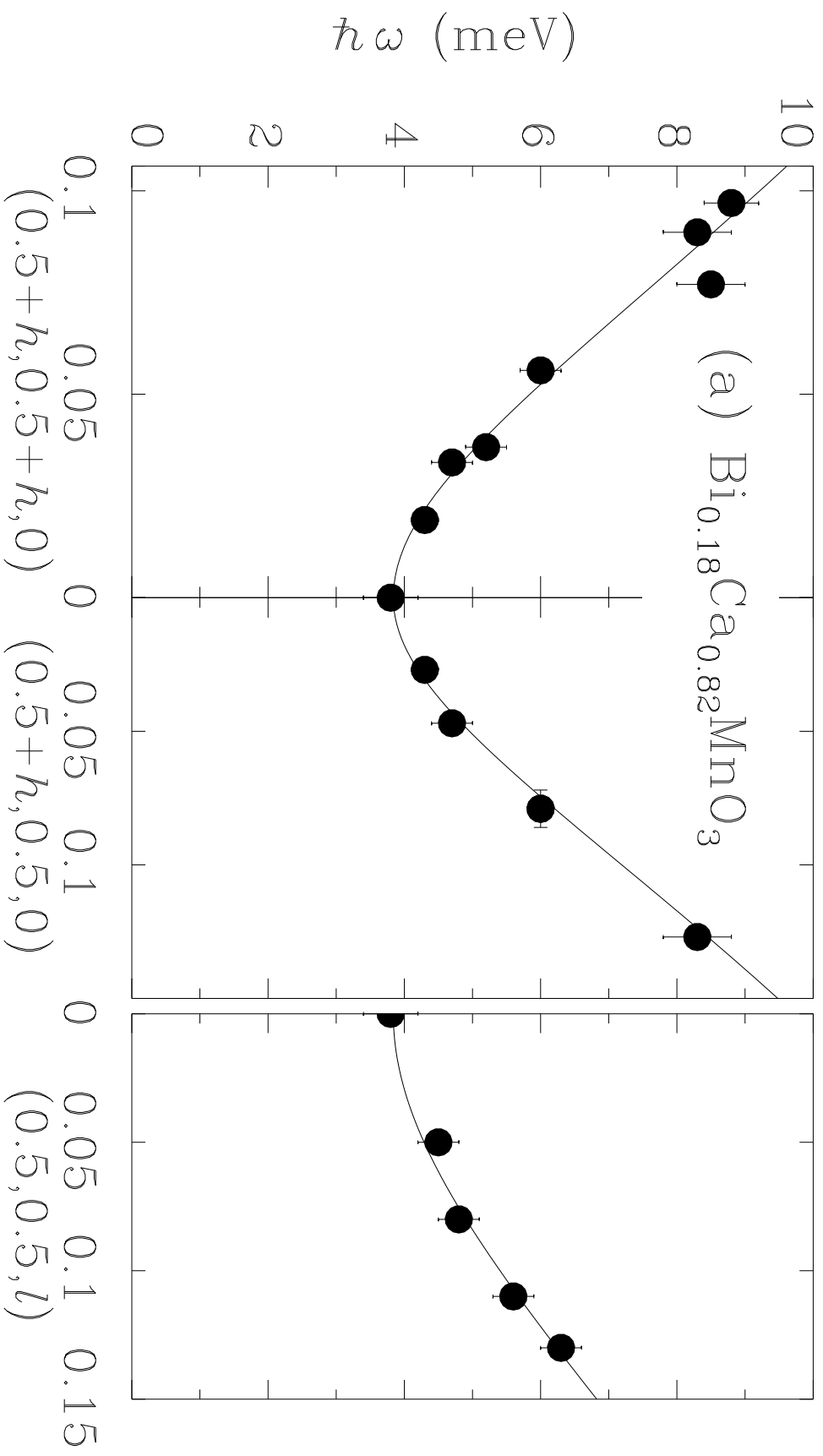


Fig. 2(upper frames), Wei Bao et al.



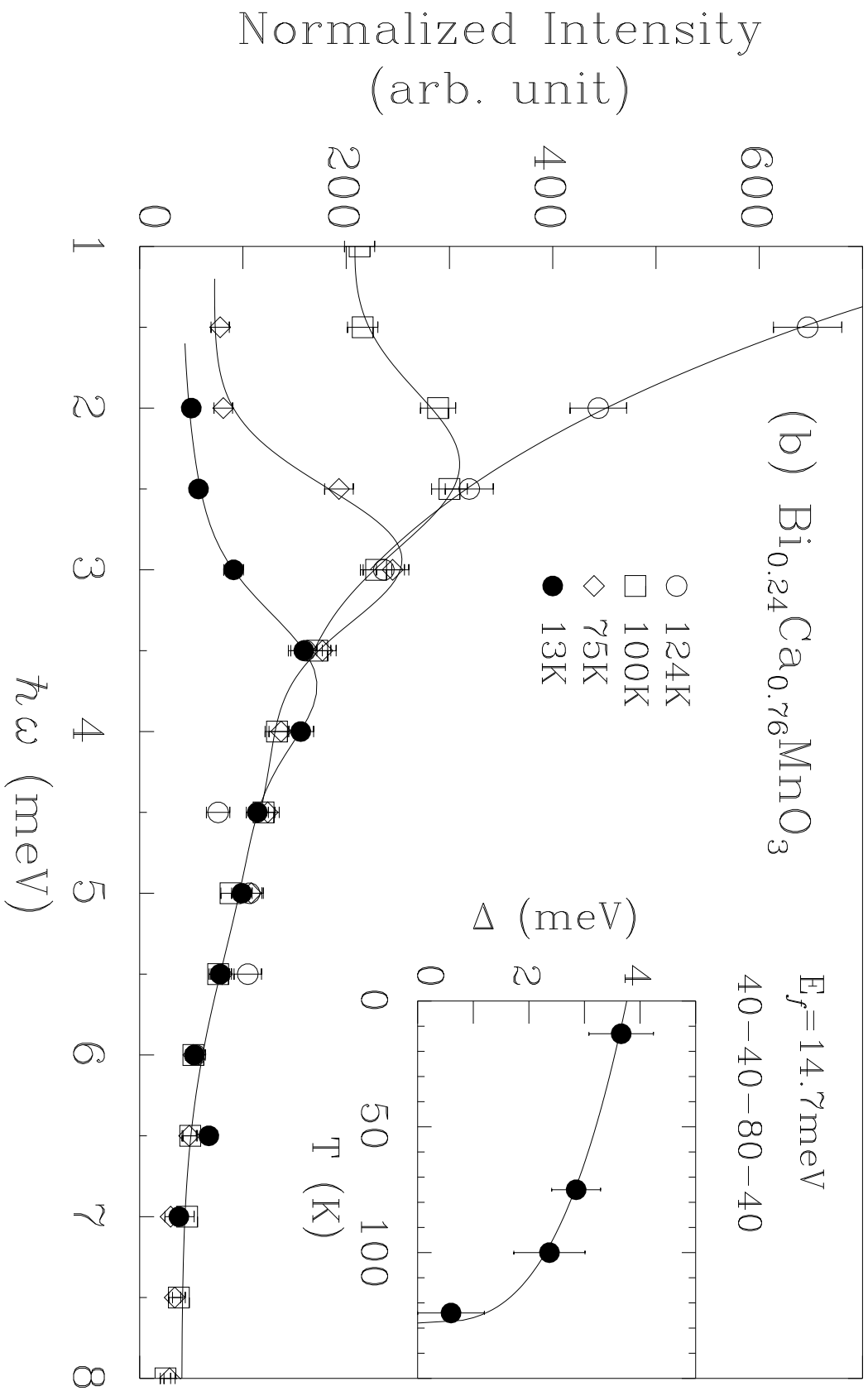


Fig. 3, Wei Bao et al.

